# Cooperative Positioning System for Industrial IoT via mmWave Device-to-Device Communications

Yi Lu, Mike Koivisto, Jukka Talvitie, Elizaveta Rastorgueva-Foi, Mikko Valkama, and Elena Simona Lohan
*Department of Electrical Engineering, Tampere University, Finland*
{yi.lu, mike.koivisto, jukka.talvitie, elizaveta.rastorgueva-foi, mikko.valkama, elena-simona.lohan}@tuni.fi

***Abstract*—The millimeter wave (mmWave) device-to-device air interface not only supports a direct wireless connectivity among devices, but it also offers an improved beamforming capability to obtain the direction information among the vehicles and devices for positioning. Both features serve as the key physical layer components for communications and positioning in the industrial Internet of things (IIoT) systems. Exploiting both accurate beamforming and wide bandwidth in a mmWave network, high-accuracy positioning is achievable, which can be then facilitated for location-aware communications, for instance. However, the uncertainty of anchors' locations in the industrial environment highly degrades the achievable positioning accuracy if left without proper consideration. In order to resolve such challenge, this paper presents a cooperative positioning system (CPS), where the locations of all the vehicles and anchors can be jointly estimated based on acquired location-related measurements (LRMs). Furthermore, the positioning performance is evaluated under random trajectories and different geometric relationships between the vehicles and the anchors. We show that, the proposed positioning solution is capable of resolving the aforementioned challenge by simultaneously tracking the mobile vehicles while mapping the locations of the static anchors. Utilizing the LRMs from both time and angular domains, the achieved positioning accuracy in both 2D and vertical plane is demonstrated based on extensive numerical simulations. Last but not least, the impact of different numbers of the mobile vehicles on the overall positioning performance is also investigated.**

***Index Terms*—Cooperative positioning, extended Kalman filter, industrial IoT, millimeter wave device-to-device communications, NR sidelink, simultaneous localization and mapping**

## I. Introduction

With the growing employment of Internet of things (IoT) technology in various industry verticals [1], an increasing amount of wireless-enabled vehicles and sensors are to be deployed in the typical industrial environments, such as harbor area and warehouses for tasks like data collection and environment monitoring. Therefore, an enhanced inter-connectivity among the vehicles via the device-to-device (D2D) air interface, i.e., the sidelink, is required for seamless communications and data exchange. As studied in [2], the new radio (NR) sidelink, not only facilitates such inter-connectivity that can be exploited for both communications and positioning, but it also plays an important role in ultimately enabling a wireless-controlled industrial Internet of things (IIoT) system with connected vehicles especially in the context of the proximity-based services (ProSe) and the vehicle-to-everything (V2X) services [3].

Although the advantages of the sidelink for communications were studied, for instance, in [4], its potential benefits for positioning have not been widely investigated especially in the millimeter wave (mmWave) networks featured with beamforming capability. In contrast to a typical cellular scenario [5], a potential and crucial challenge from the positioning perspective remains, i.e., the location uncertainty of the anchors. Indeed, the location information of the anchors may not be precisely known as usual due to a frequent deployment and re-deployment of the anchors in order to enable wireless communications in certain area of the industrial environment. In such context, we propose a cooperative positioning system (CPS) that builds on a Bayesian framework, in which, the locations of all the vehicles and anchors can be jointly estimated based on the acquired location-related measurements (LRMs) via signaling through NR sidelink. The corresponding performance in both 2D and vertical plane is evaluated via extensive ray-tracing based numerical simulations.

In terms of the related works on cooperative positioning, the authors in [6] derived the positioning error bound for mobile agents based on a single type of LRMs, such as received signal strength (RSS), time of arrival (ToA) and angle of arrival (AoA), and discussed the feasibility of acquiring LRMs by utilizing different technologies, such ultra-wideband (UWB) and acoustic media. However, the achievable positioning accuracy by collectively utilizing different types of LRMs (e.g., RSS+AoA) were not discussed therein. Due to the high temporal resolution, the authors in both [7] and [8] adopted the UWB to verify the positioning performance experimentally. In particular, the authors in [7] proposed a robust algorithm by mapping the graphical model into the network topology, yielding small communication overhead and good positioning accuracy. Moreover, an anchorless and cooperative tracking algorithm was proposed in [8] where the multi-path components were utilized for positioning with an available 2D floorplan. Nevertheless, the vertical accuracy which is crucial for certain industrial use cases was not characterized therein. Last but not least, the cooperative positioning was addressed using the set-theoretic estimation methods in [9].

Finally, the main contributions of the proposed positioning framework in this paper are summarized as:

1) By categorizing the involved vehicles and devices into

This work was financially supported by the Academy of Finland, under the projects ULTRA (328226, 328214) and FUWIRI (319994), and the Finnish Funding Agency for Innovation under the project 5G VIIMA. Online videos are available at: https://research.tuni.fi/wireless/research/positioning/cps-d2d/

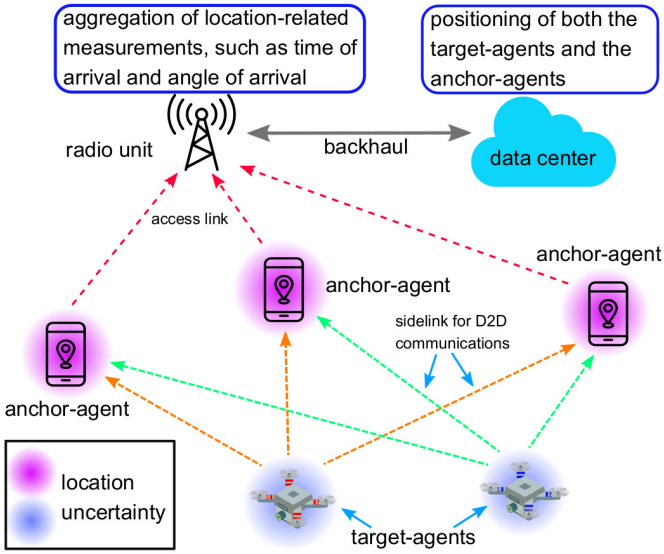


Fig. 1: In the considered positioning framework, the anchor-agents first estimate the location-related measurements (LRMs) based on the received pilot signal from the target-agents via the established sidelink (shown as green and orange dashed lines), after which these LRMs are first communicated to and aggregated at the radio unit (RU), and then fused into the location estimates of both anchor-agents and target-agents at the data center (or locally at the RU [10]) in a sequential manner by employing the proposed extended Kalman filter (EKF)-based approach. The locations of neither the target-agents nor the anchor-agents are perfectly known, the uncertainty is indicated by the blue and magenta shaded circles.

two kinds (targets and anchors) depending on their mobility and functionality, the LRMs are needed only over a subset of the overall D2D connections (i.e., less data) compared to aforementioned works;

2) By fusing the acquired LRMs individually and collectively[1], we provide an extended Kalman filter (EKF)-based formulation that enables the positioning and tracking of both the targets and the anchors in 3D;
3) With two sets of anchor deployment, we evaluate the impact on positioning due to different geometric relationships between the targets and the anchors;
4) Last but not least, we investigate the positioning performance of the proposed algorithm when considering different number of targets.

## II. System Models and Descriptions

### A. The cooperative positioning system (CPS)

In this paper, the considered wireless IIoT system is composed of various aerial or ground vehicles and sensor devices, which we refer to as *agents* that are capable of transmitting and receiving radio signals. As illustrated in Fig. 1, two types of agents are considered herein, one refers to the target-agent (T-agent), e.g., unmanned aerial vehicles, which possesses high mobility in order to perform certain tasks, such as environment monitoring and video surveillance. Another type of an agent is the anchor-agent (A-agent), such as the sensor device, which maintains a low mobility for most of the time serving as anchors. Under such context, the core objective of the proposed CPS is to track the moving T-agents while mapping the locations of the static A-agents, thus establishing the simultaneous localization and tracking (SLAT) approach.

In terms of beamforming capability, we assume that all the A-agents are equipped with a directional antenna, such as a uniform rectangle array (URA) in order to estimate the angle-domain LRMs (i.e., the AoA) when periodically receiving the transmitted pilot signals (e.g., the sidelink synchronization signals [11]) from the T-agents. In particular, the pilot signals employ the orthogonal frequency division multiplex (OFDM) waveforms, and the othogonal frequency division multiple access (OFDMA) is adopted as the resource assignment scheme among the T-agents and A-agents. Thereafter, the estimated LRMs at each A-agent are sent to the radio unit (RU) and finally received via backhaul at the data center of the network (i.e., the edge or cloud server) for cooperative positioning.

### B. Radio signal and channel models

We continue with the theoretical characterization of the considered signal and channel models. Specifically, at an arbitrary time instant $i$, the $k$th T-agent, where $k \in \mathcal{K} = \{1, 2, \cdots, K\}$, transmits sidelink physical signals [11] by means of OFDM. In this particular work, all the T-agents are equipped with omni-directional antennas (an array with a single antenna element). Hence, we have a $N_R \times 1$ channel matrix for each pair of T-agent and A-agent, where $N_R$ refers to the number of antenna elements at the receiver side (A-agent). Furthermore, we denote the transmitted OFDM symbol at the $p$th sub-carrier as $s_k[p,i] \in \mathbb{C}$. After passing through a line-of-sight (LoS)-dominant mmWave multi-path channel, the transmitted signals are received at the A-agents via a beam sweeping process[2].

The received frequency-domain complex symbol $r_m^{(q,k)}[p,i]$ at the $m$th A-agent, where $m \in \mathcal{M} = \{1, 2, \cdots, M\}$ from the $k$th T-agent at the $i$th time instant and the $p$th sub-carrier through the $q$th analog beamformer is expressed as

$$r_m^{(q,k)}[p,i] = \left(\boldsymbol{w}_m^{(q)}[i]\right)^{\mathrm{H}} \left(\boldsymbol{\Lambda}_m[p] s_k[p,i] + \boldsymbol{n}[p,i]\right), \quad (1)$$

where $\boldsymbol{n}[p,i] \sim \mathcal{CN}\left(\mathbf{0}, \sigma_n^2 \mathbf{I}_{N_R}\right)$ refers to the complex-Gaussian noise with a power density of $\sigma_n^2$ imposed on overall $N_R$ antenna elements. Furthermore, the $q$th beamformer $\boldsymbol{w}_m^{(q)}[i] \in \mathbb{C}^{N_R \times 1}$ can be constructed, but not limited to, via phase-shifters according to certain spatial angles in the utilized codebook. In addition, the identity matrix and Hermitian operation are denoted as $\mathbf{I}$ and $(\cdot)^{\mathrm{H}}$, respectively.

The channel matrix of each sub-carrier, denoted as $\boldsymbol{\Lambda}_m[p] \in \mathbb{C}^{N_R \times N_T}$ (note that $N_T = 1$ in this work) can be written as

$$\begin{aligned} \boldsymbol{\Lambda}_m[p] &= \boldsymbol{A}\boldsymbol{\Gamma}[p] \\ &= \sum_{l=0}^{L-1} \boldsymbol{b}_{\mathrm{URA}}\left(\phi_l\right) \gamma_l e^{-j2\pi f_{\mathrm{sc}} p \tau_l}, \end{aligned} \quad (2)$$

[1]'Individually' means utilizing of one type of LRMs, e.g., only ToA; 'Collectively' means more than one type of LRMs are applied, e.g., ToA+AoA.

[2]The beam sweeping refers to one beam management process [12], where multiple beamformers, i.e., beam steering vectors are applied to acquire the received signals from different directions.

where $L$ is the overall number of propagation paths and the channel state vector $\mathbf{\Gamma}[p] \in \mathbb{C}^{L\times 1}$ is described as

$$\mathbf{\Gamma}[p] = \left[\gamma_0 e^{-j2\pi f_{\text{sc}} p\tau_0}, \cdots, \gamma_{L-1} e^{-j2\pi f_{\text{sc}} p\tau_{L-1}}\right]^T, \quad (3)$$

where the index of active sub-carrier $p \in \mathcal{P} = \{1, \cdots, P\}$ and $f_{\text{sc}}$ is the sub-carrier spacing. The array response matrix in (2) is represented as $\boldsymbol{A} \in \mathbb{C}^{N_R\times L} = [\boldsymbol{b}_{\text{URA}}(\phi_0), \cdots, \boldsymbol{b}_{\text{URA}}(\phi_{L-1})]$. Specifically, $\boldsymbol{b}_{\text{URA}}(\phi_l) \in \mathbb{C}^{N_R\times 1}$ refers to the URA response at the spatial angle $\phi_l \triangleq (\theta_l, \varphi_l)$, and $\gamma_l$ is the complex channel coefficient including the pathloss of the $l$th path with a propagation delay of $\tau_l$. Moreover, $\boldsymbol{b}_{\text{URA}}(\phi_l)$ is a combination of two uniform linear array (ULA) responses

$$\boldsymbol{b}_{\text{URA}}(\phi_l) = \sqrt{\beta_0(N_R, \phi_l)}\boldsymbol{a}_{\text{ULA}}(\varphi_l) \otimes \boldsymbol{a}_{\text{ULA}}(\theta_l|\varphi_l), \quad (4)$$

where $\otimes$ denotes the Kronecker product and the scaling factor $\beta_0(N_R, \phi_l)$ represents the array gain as a function of the overall number of antenna elements $N_R$ as well as the spatial angle pair $\phi_l$. As defined previously, the angle pair $\phi_l$ consists of the azimuth angle $\theta_l$ as well as the elevation angle $\varphi_l$, and together, they define a spatial direction in a 3D environment. Hence, the individual normalized ULA responses are given as

$$\begin{aligned}\boldsymbol{a}_{\text{ULA}}(\varphi_l) &= \frac{e^{-j\pi\sin(\varphi_l)\left[-\frac{N_{\text{el}}-1}{2}, \cdots, \frac{N_{\text{el}}-1}{2}\right]^T}}{\sqrt{N_{\text{el}}}},\\ \boldsymbol{a}_{\text{ULA}}(\theta_l|\varphi_l) &= \frac{e^{-j\pi\cos(\varphi_l)\sin(\theta_l)\left[-\frac{N_{\text{az}}-1}{2}, \cdots, \frac{N_{\text{az}}-1}{2}\right]^T}}{\sqrt{N_{\text{az}}}},\end{aligned} \quad (5)$$

where $N_{\text{el}}$ and $N_{\text{az}}$ represent the dimensions of the URA, such that $N_R = N_{\text{el}}N_{\text{az}}$. In case of a $8 \times 8$ URA, $N_{\text{el}} = N_{\text{az}} = 8$.

### C. The location-related measurements (LRMs)

Denoting the locations of the $k$th T-agent and the $m$th A-agent as $\mathbf{P}_{\text{T},k}[i] = [x_{\text{T},k}, y_{\text{T},k}, z_{\text{T},k}]^T$ and $\mathbf{P}_{\text{A},m}[i] = [x_{\text{A},m}, y_{\text{A},m}, z_{\text{A},m}]^T$, respectively, we formulate all the desired time-domain and the angle-domain LRMs as

$$\begin{aligned}\hat{\tau}_m^{(k)} &= \tau_m^{(k)} + n_{\tau,m}^{(k)} = \|\mathbf{P}_{\text{T},k} - \mathbf{P}_{\text{A},m}\|/c + n_{\tau,m}^{(k)},\\ \hat{\Delta\tau}_m^{(k)} &= \Delta\tau_m^{(k)} + n_{\Delta\tau,m}^{(k)}\\ &= \|\mathbf{P}_{\text{T},k} - \mathbf{P}_{\text{A},m}\|/c - \|\mathbf{P}_{\text{T},k} - \mathbf{P}_{\text{A},1}\|/c + n_{\Delta\tau,m}^{(k)},\\ \hat{\varphi}_m^{(k)} &= \varphi_m^{(k)} + n_{\varphi,m}^{(k)}\\ &= \arcsin\left(\Delta z_m^{(k)}/\|\mathbf{P}_{\text{T},k} - \mathbf{P}_{\text{A},m}\|\right) + n_{\varphi,m}^{(k)},\\ \hat{\theta}_m^{(k)} &= \theta_m^{(k)} + n_{\theta,m}^{(k)}\\ &= \text{atan}_2\left(\Delta y_m^{(k)}, \Delta x_m^{(k)}\right) + n_{\theta,m}^{(k)},\end{aligned} \quad (6)$$

where the considered LRMs consist of ToA $\hat{\tau}_m^{(k)}[i]$, time difference of arrival (TDoA) $\hat{\Delta\tau}_m^{(k)}[i]$, elevation AoA $\hat{\varphi}_m^{(k)}[i]$ and azimuth AoA $\hat{\theta}_m^{(k)}[i]$, and the time index in (6) are omitted for simplicity. Furthermore, $c$ is the speed of light, $\Delta x_m^{(k)} = x_{\text{T},k} - x_{\text{A},m}$, $\Delta y_m^{(k)} = y_{\text{T},k} - y_{\text{A},m}$, $\Delta z_m^{(k)} = z_{\text{T},k} - z_{\text{A},m}$. Additionally, the inverse sine function and four-quadrant inverse tangent function are denoted as arcsin and $\text{atan}_2$, respectively.

More importantly, we model all the LRMs noises in (6) as unbiased additive Gaussian white noise having the variance that is bounded by the established Cramér-Rao lower bound (CRLB) [13, Ch. 3]. For instance, we express the CRLB of ToA and elevation AoA as follows

$$\sigma^2_{\tau,m,k}[i] \geq \frac{3}{8\pi^2 f_{\text{sc}}^2 \text{SNR}_m^{(k)}[i] M_p(M_p+1)(2M_p+1)}, \quad (7)$$

$$\sigma^2_{\varphi,m,k}[i] \geq \frac{6}{N_{\text{el}}\left(N_{\text{el}}^2-1\right)\text{SNR}_m^{(k)}[i]\ \pi^2\cos^2\left(\varphi_m^{(k)}[i]\right)}, \quad (8)$$

where $M_p = \frac{P-1}{2}$, $P$ is the overall number of active sub-carriers. We see that both CRLB are a function of several parameters, such as the signal bandwidth, $B_w = f_{\text{sc}}P$, the signal-to-noise ratio (SNR), $\text{SNR}_m^{(k)}[i]$, the number of antenna elements, $N_{\text{el}}$ and the true AoA, $\varphi_m$. Additionally, the TDoA noise model can be computed as $\sigma^2_{\Delta\tau,m}[i] = \sigma^2_{\tau,m}[i] - \sigma^2_{\tau,1}[i]$[3], whereas the azimuth AoA shares the same formulation as (8) except that the term $N_{\text{el}}$ shall be swapped to $N_{\text{az}}$.

Of all the parameters, the SNR remains significant since it is a time-variant variable due to the movement of all the T-agents and its value determines the ultimate LRMs' accuracy. After beam sweeping, the obtained SNR is expressed as

$$\text{SNR}_m^{(k)}[i] = \frac{\max\left(\mathbf{B}_m^{(k)}[i]\right)}{P_n}, \quad (9)$$

where $P_n$ refers to the noise power over the total signal bandwidth, and the obtained beam reference signal received power (B-RSRP) vector is denoted as $\mathbf{B}_m^{(k)}[i] \in \mathbb{R}^{Q\times 1}$ where $Q$ is the overall number of the beamformers in the codebook, and the $q$th B-RSRP $\text{B}_m^{(q,k)}[i]$ is calculated based on (1)

$$\text{B}_m^{(q,k)}[i] = \frac{1}{P}\sum_{p=1}^{P}|r_m^{(q,k)}[p,i]|^2, \quad (10)$$

that is essentially the average power over all the active sub-carriers.

## III. Cooperative positioning via EKF

The proposed CPS for positioning of T-agents and A-agents are building on an EKF that is widely applied for positioning in works such as [8]. The choice of an EKF is determined by its flexibility in dealing with the non-linear state transition or measurement models. The proposed EKF is formulated according to [14] as

$$\begin{aligned}\text{state transition model}: \mathbf{s}[i] &= \mathbf{F}\mathbf{s}[i-1] + \mathbf{u}[i]\\ \text{measurement model}: \mathbf{y}[i] &= \mathbf{h}\left(\mathbf{s}[i]\right) + \mathbf{w}[i],\end{aligned} \quad (11)$$

where $\mathbf{y}[i]$ represents the LRMs which are facilitated as the measurements in the EKF, and $\mathbf{s}[i]$ refers to the time-varying state vector[4] that contains the information of both T-agents and A-agents such as

$$\mathbf{s} = \left[\mathbf{s}_{\text{T},1}^T, \cdots, \mathbf{s}_{\text{T},K}^T, \mathbf{P}_{\text{A},1}^T, \cdots, \mathbf{P}_{\text{A},M}^T\right]^T, \quad (12)$$

[3]The ToA noise statistics of reference A-agent is denoted as $\sigma^2_{\tau,1}[i]$.

[4]Thereafter, we drop the involved time index $i$ for simplicity of the notation.

**Algorithm 1:** EKF-based cooperative positioning

At time index $i = 0$, initialize the state $\mathbf{s}$, covariance $\mathbf{\Sigma}$, process noise covariance $\mathbf{Q}$ according to Section IV-A

**for** $i = 1, \cdots, T$ **do**

Generate the LRMs vector $\mathbf{y}[i]$ and compute the corresponding measurement noise covariance matrix $\mathbf{R}[i]$

Calculate the Jacobian matrix according to, e.g., (16)

Implement the EKF equations [14]

**Prediction**:

state $\hat{\mathbf{s}}^{-}[i] = \mathbf{F}\hat{\mathbf{s}}[i-1]$

state covariance $\hat{\mathbf{\Sigma}}^{-}[i] = \mathbf{F}\hat{\mathbf{\Sigma}}[i-1]\mathbf{F}^{T} + \mathbf{Q}[i]$

**Kalman gain**:

$\mathbf{K}[i] = \hat{\mathbf{\Sigma}}^{-}[i]\mathbf{H}^{T}[i]\left(\mathbf{H}[i]\hat{\mathbf{\Sigma}}^{-}[i]\mathbf{H}^{T}[i] + \mathbf{R}[i]\right)^{-1}$

**Correction/update**:

$\hat{\mathbf{s}}[i] = \hat{\mathbf{s}}^{-}[i] + \mathbf{K}[i]\left(\mathbf{y}[i] - \mathbf{h}\left(\hat{\mathbf{s}}^{-}[i]\right)\right)$

$\hat{\mathbf{\Sigma}}[i] = \left(\mathbf{I} - \mathbf{K}[i]\mathbf{H}[i]\right)\hat{\mathbf{\Sigma}}^{-}[i]$

**end**

TABLE I: The number of available LRMs as a function of the number of T-agents $K$ and A-agents $M$ for each considered measurement type

| Measurement type | Number of available LRMs, $N$ |
|---|---|
| ToA, $\tau$ | $MK$ |
| TDoA, $\Delta\tau$ | $(M-1)K$ |
| AoA, $\phi$ | $2MK$ |
| ToA+AoA, $\tau$+$\phi$ | $3MK$ |
| TDoA+AoA, $\Delta\tau$+$\phi$ | $(3M-1)K$ |

in which, the state vector of the $k$th T-agent is given as

$$\mathbf{s}_{\mathrm{T},k} = \left[\mathbf{p}_{\mathrm{T},k}^{T}, \mathbf{v}_{\mathrm{T},k}^{T}, \mathbf{a}_{\mathrm{T},k}^{T}\right]^{T}, \tag{13}$$

where $\mathbf{v}_{\mathrm{T},k}^{T} = \left[v_x^{\mathrm{T},k}, v_y^{\mathrm{T},k}, v_z^{\mathrm{T},k}\right]$ and $\mathbf{a}_{\mathrm{T},k}^{T} = \left[a_x^{\mathrm{T},k}, a_y^{\mathrm{T},k}, a_z^{\mathrm{T},k}\right]$ denote the state of target velocity and acceleration, respectively. Although only the locations of the A-agents are considered in the state vector, their velocity and acceleration can also be included to enable the tracking of certain movements.

Moreover, the process noise vector is denoted as $\mathbf{u} \sim \mathcal{N}\left(\mathbf{0}_{9K+3M}, \mathbf{Q}\right)$ where $\mathbf{0}_{9K+3M}$ is a zero-vector with a dimension of $9K+3M$. Together with the linear state transition matrix $\mathbf{F}$ and the state covariance matrix $\mathbf{\Sigma}$, we have

$$\mathbf{Q} = \begin{bmatrix} \mathbf{Q}_{\mathrm{T}} & \mathbf{0} \\ \mathbf{0} & \mathbf{Q}_{\mathrm{A}} \end{bmatrix}, \mathbf{F} = \begin{bmatrix} \mathbf{F}_{\mathrm{T}} & \mathbf{0} \\ \mathbf{0} & \mathbf{F}_{\mathrm{A}} \end{bmatrix}, \mathbf{\Sigma} = \begin{bmatrix} \mathbf{\Sigma}_{\mathrm{T}} & \mathbf{0} \\ \mathbf{0} & \mathbf{\Sigma}_{\mathrm{A}} \end{bmatrix}, \tag{14}$$

where $\mathbf{Q}_{\mathrm{T}} \in \mathbb{R}^{9K\times 9K}$, $\mathbf{Q}_{\mathrm{A}} \in \mathbb{R}^{3M\times 3M}$, $\mathbf{F}_{\mathrm{T}} \in \mathbb{R}^{9K\times 9K}$, $\mathbf{F}_{\mathrm{A}} \in \mathbb{R}^{3M\times 3M}$, $\mathbf{\Sigma}_{\mathrm{T}} \in \mathbb{R}^{9K\times 9K}$ and $\mathbf{\Sigma}_{\mathrm{A}} \in \mathbb{R}^{3M\times 3M}$ are the process noise covariance matrix, the linear state transition matrix and state covariance matrix of the considered T-agents and A-agents, respectively. In particular, both $\mathbf{Q}_{\mathrm{T}}$ and $\mathbf{F}_{\mathrm{T}}$ are block diagonal matrices that consist of the corresponding matrix of each individual T-agent, i.e., $\mathbf{Q}_{\mathrm{T}} = \mathrm{blkdiag}\left(\mathbf{Q}_{\mathrm{T},1}, \cdots, \mathbf{Q}_{\mathrm{T},K}\right)$ and $\mathbf{F}_{\mathrm{T}} = \mathrm{blkdiag}\left(\mathbf{F}_{\mathrm{T},1}, \cdots, \mathbf{F}_{\mathrm{T},K}\right)$. Assuming a constant acceleration between consecutive states, we have [15]

$$\begin{aligned} \mathbf{F}_{\mathrm{T},k} &= \begin{bmatrix} 1 & \Delta t & \frac{\Delta t^2}{2} \\ 0 & 1 & \Delta t \\ 0 & 0 & 1 \end{bmatrix} \otimes \mathbf{I}_{3\times 3}, \\ \mathbf{Q}_{\mathrm{T},k} &= \sigma_{q,k}^2 \begin{bmatrix} \frac{\Delta t^5}{20} & \frac{\Delta t^4}{8} & \frac{\Delta t^3}{6} \\ \frac{\Delta t^4}{8} & \frac{\Delta t^3}{3} & \frac{\Delta t^2}{2} \\ \frac{\Delta t^3}{6} & \frac{\Delta t^2}{2} & \Delta t \end{bmatrix} \otimes \mathbf{I}_{3\times 3}, \end{aligned} \tag{15}$$

where $\Delta t$ denotes the time interval between two consecutive time steps, and $\sigma_{q,k}^2$ refers to the process noise variance of the acceleration of the $k$th T-agent. For the A-agents, $\mathbf{F}_{\mathrm{A}} = \mathbf{I}_{3M\times 3M}$ and $\mathbf{Q}_{\mathrm{A}} = \mathbf{I}_{3M\times 3M}\sigma_{q,\mathrm{A}}^2$. Similarly, we have the initial state covariance of both agents as the block diagonal matrices as well where $\mathbf{\Sigma}_{\mathrm{T}} = \mathrm{blkdiag}\left(\mathbf{\Sigma}_{\mathrm{T},1}, \cdots, \mathbf{\Sigma}_{\mathrm{T},K}\right)$, where $\mathbf{\Sigma}_{\mathrm{T},k} = \mathrm{blkdiag}\left(\mathbf{\Sigma}_{\mathrm{P},k}, \mathbf{\Sigma}_{\mathrm{v},k}, \mathbf{\Sigma}_{\mathrm{a},k}\right)$ and for the A-agents $\mathbf{\Sigma}_{\mathrm{A}} = \mathrm{blkdiag}\left(\mathbf{\Sigma}_{\mathrm{A},1}, \cdots, \mathbf{\Sigma}_{\mathrm{A},M}\right)$ in which $\mathbf{\Sigma}_{\mathrm{A},m} = \mathrm{diag}\left(\sigma_x^2, \sigma_y^2, \sigma_z^2\right)$.

Furthermore, we denote the measurement noise vector as $\mathbf{w} \sim \mathcal{N}\left(\mathbf{0}_N, \mathbf{R}\right)$ where $N$ is the overall number of available LRMs. In the case where only the ToA measurements are available, the number of LRMs is equal to the number of A-agents, i.e., $N = M$. Therefore, the measurement noise covariance matrix $\mathbf{R}_\tau \in \mathbb{R}^{MK\times MK} = \mathrm{blkdiag}\left(\mathbf{R}_\tau^{(1)}, \cdots, \mathbf{R}_\tau^{(K)}\right)$ in which, $\mathbf{R}_\tau^{(k)} = \mathrm{diag}\left(\sigma_{\tau,1,k}^2, \cdots, \sigma_{\tau,M,k}^2\right)$. The overall number of LRMs as a function of the number of T-agents and A-agents is given in Table I, from which, we see that the overall number of LRMs is larger when utilizing both time- and angle-domain LRMs, which would be beneficial to the performance of CPS, as will be shown in Section IV-D. Furthermore, the measurement function $\mathbf{h}\left(\cdot\right)$ in (11) for all types of LRMs has been explicitly given in (6) from which the Jacobian matrix is computed. Taking as a concrete example the case when only ToA measurement are utilized, the Jacobian matrix $\mathbf{H}_\tau \in \mathbb{R}^{MK\times(9K+3M)}$ can be written as

$$\mathbf{H}_\tau = \begin{bmatrix} \mathbf{H}_{\tau,\mathrm{T}}^{(1)} & \mathbf{0} & \cdots & \mathbf{0} & \mathbf{H}_{\tau,\mathrm{A}}^{(1)} \\ \mathbf{0} & \mathbf{H}_{\tau,\mathrm{T}}^{(2)} & & \vdots & \mathbf{H}_{\tau,\mathrm{A}}^{(2)} \\ \vdots & & \ddots & \mathbf{0} & \vdots \\ \mathbf{0} & \cdots & \mathbf{0} & \mathbf{H}_{\tau,\mathrm{T}}^{(K)} & \mathbf{H}_{\tau,\mathrm{A}}^{(K)} \end{bmatrix}, \tag{16}$$

where $\mathbf{H}_{\tau,\mathrm{T}}^{(k)} \in \mathbb{R}^{M\times 9}$ and $\mathbf{H}_{\tau,\mathrm{A}}^{(k)} \in \mathbb{R}^{M\times 3M}$ refer to the Jacobian matrix of the $k$th T-agent, where the partial derivatives are taken with respect to (w.r.t.) the variables of T-agent and A-agent, respectively. Additionally, $\mathbf{H}_{\Delta\tau}$, $\mathbf{H}_{\phi}$, $\mathbf{H}_{\tau+\phi}$ and $\mathbf{H}_{\Delta\tau+\phi}$ are constructed in the same manner as (16), and they are evaluated at the a prior mean $\hat{\mathbf{s}}^{-}$ which is shown in Algorithm 1 where the proposed cooperative positioning EKF is briefly summarized. Moreover, the specific Jacobian matrices of $\mathbf{H}_{\tau,\mathrm{T}}^{(k)}$ and $\mathbf{H}_{\phi,\mathrm{T}}^{(k)}$ can be found in [15, Section IV].

## IV. Numerical simulations and results analysis

### A. Initialization

For the numerical evaluation of the proposed positioning algorithm, the EKF state $\mathbf{s}$ was initialized with random

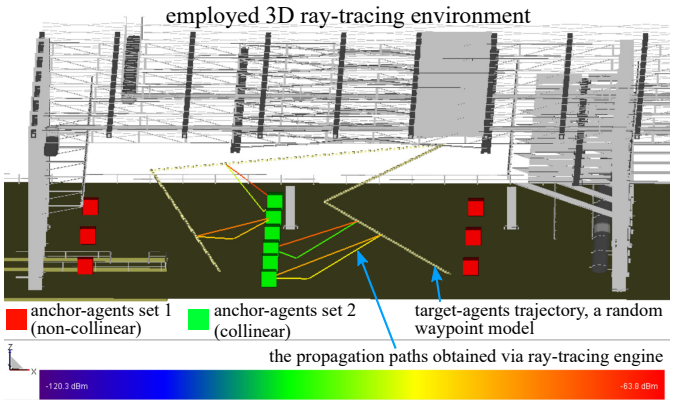


Fig. 2: The ray-tracing enabled 3D industrial environment [16] with two practical A-agents sets, i.e., non-collinear (set 1) deployment in red and collinear (set 2) deployment in green. An example of T-agent trajectory based on a 3D random waypoint (RWP) model in plotted in light yellow.

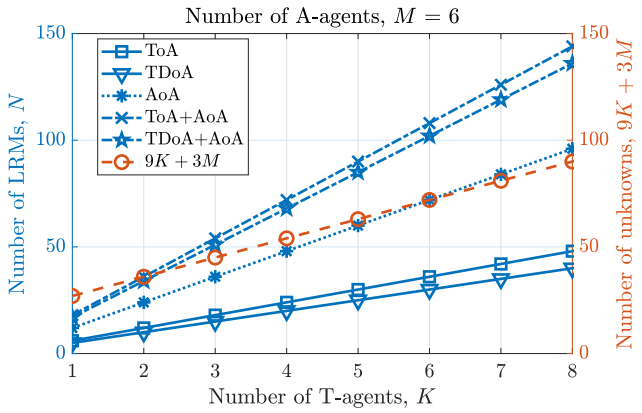


Fig. 3: The overall number of LRMs (left y-axis) and the overall number of unknowns (right y-axis) as a function of the number of considered T-agents with the number of considered A-agents fixed at $M = 6$. The formula of calculating the number of LRMs are given in Table I.

T-agent locations that are normally distributed w.r.t. the true locations and with standard deviation of one meter in all directions, whereas the velocities and accelerations are set to zeros. Consequently, the initial state covariance matrix is given as $\mathbf{\Sigma}_{\mathrm{T},k} = \mathrm{blkdiag}\left(\mathbf{I}_{3\times 3}, \mathbf{\Sigma}_{\mathrm{v},k}, \mathbf{\Sigma}_{\mathrm{a},k}\right)$ in which $\mathbf{\Sigma}_{\mathrm{v},k} = \mathrm{diag}\left(\left(v_x^{\mathrm{T},k}\Delta t\right)^2, \left(v_y^{\mathrm{T},k}\Delta t\right)^2, \left(v_z^{\mathrm{T},k}\Delta t\right)^2\right)$ and $\mathbf{\Sigma}_{\mathrm{a},k} = \mathrm{diag}\left(\left(a_x^{\mathrm{T},k}\Delta t^2\right)^2, \left(a_y^{\mathrm{T},k}\Delta t^2\right)^2, \left(a_z^{\mathrm{T},k}\Delta t^2\right)^2\right), \forall k \in \mathcal{K}$. In addition, the locations of all the A-agents are also initialized around their true locations with a covariance $\mathbf{\Sigma}_{\mathrm{A},m} = \mathrm{diag}\left(\sigma_{\mathrm{AT}}^2, \sigma_{\mathrm{AT}}^2, \frac{\sigma_{\mathrm{AT}}^2}{\beta^2}\right)$, where $\sigma_{\mathrm{AT}}$ refers to the location uncertainty in the horizontal plane and $\beta = 10$, $\forall m \in \mathcal{M}$. Moreover, the process noise variance $\sigma_{q,k}^2$ (of T-agents) is tuned according to the maximum acceleration $|a_{\max}|$ such that $\sigma_{q,k}^2 = \left(|a_{\max}|/(6\Delta t)\right)^2$. Since the A-agents are assumed to be static in this work, the $\sigma_{q,\mathrm{A}}^2$ is set to 0.

### B. Test scenarios

The performance of the proposed CPS is evaluated using ray-tracing simulations [16] and numerical evaluations in a mmWave D2D network. In particular, six static A-agents were deployed in a 60m $\times$ 60m area according to two different sets (as depicted in Fig. 2) to evaluate the effect of different geometric relationships. Furthermore, we design the trajectories of all T-agents based on the 3D random waypoint (RWP) model [17] within the considered area, the height of each trajectory is controlled from 0.5m to 8m range, whereas the horizontal range is bounded by the borders of the warehouse. In particular, there are approximately 25 paths (including the LoS path) being generated for each pair of target-anchor at each time instant using ray-tracing simulations. For the purpose of demonstration, the LoS path together with one first-order reflection path are given as examples in Fig. 2. In addition, all the T-agents move independently along their individual trajectories. Subsequently, we summarize the relevant parameters utilized in the simulation in Table II. It is also noteworthy that with the considered parameter configurations, the theoretical maximum D2D distance in the LoS condition is more than 500m, which is enough to ensure the full radio coverage within the environment.

TABLE II: Utilized parameters in the simulation

| Parameter | Value |
|---|---|
| Carrier frequency | 26 GHz |
| Sub-carrier spacing | 60 kHz |
| Signal bandwidth | 10 MHz |
| Transmit power | 10 dBm |
| Receive beamforming gain | 18 dBi |
| EKF update time-interval | 100 ms |
| A-agents antenna | $8 \times 8$ URA |
| T-agents antenna | Omni-directional |
| A-agents height | 1.5 m |
| T-agents height | 0.5 – 8 m |
| Avg. T-agents velocity | 1.1 m/s |

### C. The number of LRMs vs the number of unknowns

Given the number of T-agents, $K$, and the number of A-agents, $M$, the number of unknowns in the estimation problem is $9K + 3M$. In particular, Fig. 3 demonstrates the number of available LRMs, $N$, as a function of $K$ in the case of six A-agents[5] when utilizing different types of LRMs. It is observed that with the increasing value of $K$, the number of both the unknowns and the LRMs increases. Nevertheless, for the considered number of T-agents, the problem is under-determined ($N < 9K + 3M$) for CPS that applies the time-domain LRMs (ToA, TDoA) and angle-domain LRMs (AoA) individually, and become over-determined ($N > 9K + 3M$) for CPS collectively utilizing the LRMs from both time- and angle-domain (ToA+AoA and TDoA+AoA). A critical case occurs when $K = 2$ and both ToA and AoA measurements are utilized, in which case, $N = 9K + 3M$. In the following subsections, we will present positioning performance under different $K$ and $M$ values.

### D. The impact of different numbers of T-agents and A-agents

To assess if the presence of more T-agents could bring practical benefits to the CPS, we first test and present the

[5]We emphasize that $M$ can be any positive integer number, and $M = 6$ is chosen here such that there is one A-agent every 25m$\times$25m area approximately.

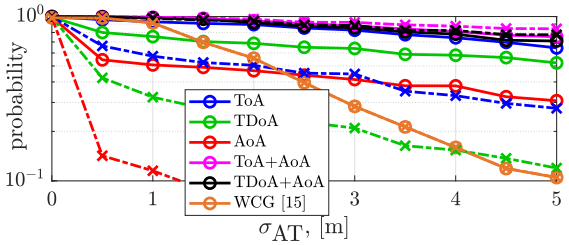


(a) Probability of 2D sub-meter accuracy in set 1 (non-collinear A-agents).

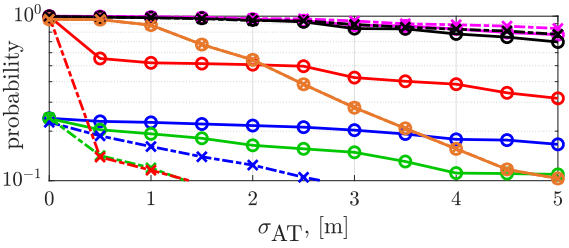


(b) Probability of 2D sub-meter accuracy in set 2 (collinear A-agents).

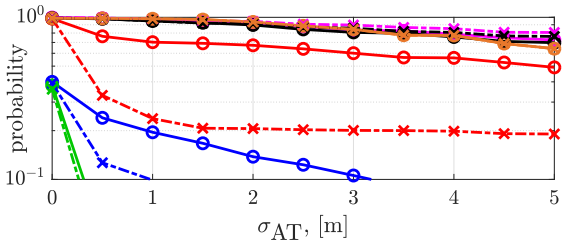


(c) Probability of vertical sub-0.2 meter accuracy in set 1 (non-collinear A-agents).

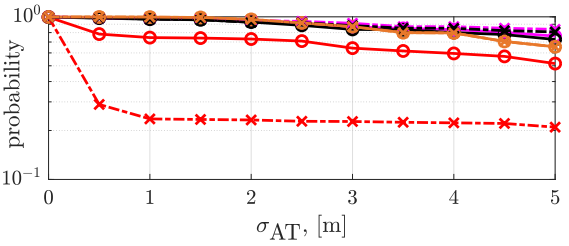


(d) Probability of vertical sub-0.2 meter accuracy in set 2 (collinear A-agents).

Fig. 4: Positioning performance of T-agents. Circle solid lines denote the positioning performance with two T-agents (two-target CPS); Cross dashed lines denote the positioning performance with one T-agent (one-target CPS).

positioning performance at $K = 1$ (one-target CPS) and $K = 2$ (two-target CPS). Moreover, we adopt the probability of sub-meter accuracy in 2D (the horizontal plane) and probability of sub-0.2 meter accuracy [18, Table 7.3.2.2-1] in vertical plane as the performance metrics. Furthermore, we perform in total 500 simulation trials with overall 1000 independent RWP trajectories generated, thus implying that two independent trajectories are generated in each simulation trial[6]. In particular, the length of each RWP trajectory is set to 2000 points with 100 ms interval.

The positioning performance of T-agents is given in Fig. 4. In terms of the performance difference between two-target CPS and one-target CPS[7], it is noticeable that when utilizing the time- and angle-domain LRMs individually, the two-target CPS outperforms the one-target CPS in both (anchor) sets and both 2D and vertical planes. However, the performance gap between two-target and one-target CPS becomes nearly invisible when collectively utilizing the LRMs from both time- and angle-domains. As expected, when utilizing different LRMs[8], both 2D and vertical positioning accuracy of the CPS that collectively utilizes the LRMs is in general higher than that of the CPS that utilizes the LRMs from a single domain. Nevertheless, it is important to note that the ToA-based two-target CPS achieves nearly equivalent 2D performance as the CPS that collectively utilizes LRMs from both domains. For both $K = 1, 2$ cases, the AoA-based CPS demonstrates a rather similar performance in both A-agents sets and both 2D and vertical planes, whereas the time-based CPS suffers a huge performance loss in set 2 (when A-agents are collinear deployed), in which a roughly $20\%$ 2D sub-meter accuracy (in Fig. 4b) and a nearly $3\%$ vertical sub-0.2 meter accuracy (invisible in Fig. 4d) are achieved.

The above observed behavior shows that the time-based CPS suffers severely from the collinear deployment (set 2), which further proves the impact on the positioning performance due to the different geometric relationships between the T-agents and the A-agents when utilizing different LRMs. Moreover, the results in Fig. 4c and Fig. 4d demonstrates that the angle-based CPS offers a much better vertical accuracy in both sets than the time-based CPS over the entire considered $\sigma_{\text{AT}}$ values. Additionally, the weighted centroid geometry (WCG) [15] that utilizes ToA+AoA is applied herein for comparison. It is seen that over the entire considered $\sigma_{\text{AT}}$ values, the WCG in general achieves a comparable vertical performance, whereas its 2D accuracy becomes much worse than the (ToA+AoA)-based CPS when $\sigma_{\text{AT}} > 1$m.

In addition to the T-agents, the positioning performance of A-agents is also obtained and presented in Fig. 5. It is to note that WCG is not included therein due to the fact that WCG is only capable of positioning the T-agents. Moreover, a comparison between Fig. 4 and Fig. 5 reveals the fact that despite slight numerical differences, the obtained performance of the A-agents is rather similar to that of the T-agents except two differences. One is that in set 2 (collinear deployment set), the A-agents (Fig. 5b and Fig. 5d) do not suffer huge accuracy loss as the T-agents (Fig. 4b and Fig. 4d) when utilizing the time-domain LRMs. The reason lies in the fact that for each A-agent in set 2, the geometric relationships between itself and other agents (i.e., the T-agents and other A-agents) are not collinear anymore. Another difference lies in the fact that the vertical performance of A-agents (Fig. 5c and Fig. 5d) is much better than that of T-agents (Fig. 4c and Fig. 4d) when utilizing time-domain LRMs.

The CPS performance is visualized and available online at: https://research.tuni.fi/wireless/research/positioning/cps-d2d/

## V. Conclusion

In this paper, we proposed and evaluated a cooperative positioning solution operating on the mmWave D2D air

[6]One out of the two RWP trajectories is selected as the trajectory of the T-agent for one-target CPS.

[7]Comparison between curves in the same colors but with different markers.

[8]Comparison between curves with the same markers but in different colors.

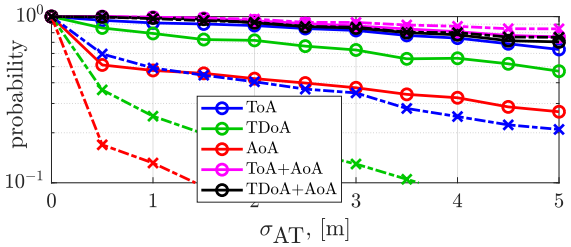


(a) Probability of 2D sub-meter accuracy in set 1 (non-collinear A-agents).

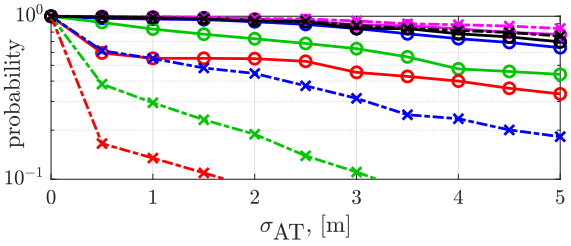


(b) Probability of 2D sub-meter accuracy in set 2 (collinear A-agents).

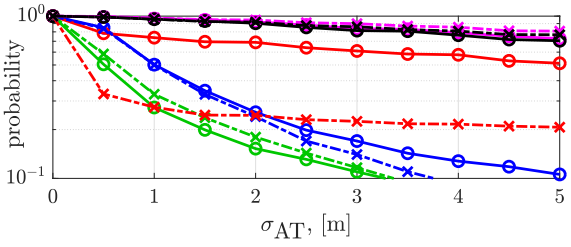


(c) Probability of vertical sub-0.2 meter accuracy in set 1 (non-collinear A-agents).

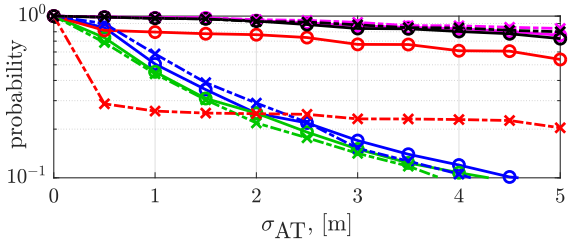


(d) Probability of vertical sub-0.2 meter accuracy in set 2 (collinear A-agents).

Fig. 5: Positioning performance of A-agents. Same as Fig. 4, circle solid lines: two-target CPS; Cross dashed lines: one-target CPS.

interface for the IIoT. The locations of all the agents (including mobile vehicles and anchor devices) can be jointly estimated, forming a SLAT-sense framework. Employing the CRLB-based LRMs from both time- and angle-domains, numerical simulations were carried out with two sets of A-agents under different geometric relationships. Our results demonstrated that the performance in both 2D and vertical plane was boosted when utilizing the LRMs collectively (i.e., time- and angle-domain LRMs together) rather than individually (i.e., either time- or angle-domain LRMs). Furthermore, compared with angle-based positioning, time-based positioning in general performed better in 2D plane and worse in vertical plane. The results also showed that the collinear geometry could severely degrade the 2D positioning performance of the T-agents rather than that of the A-agents of the CPS that utilized only time-domain LRMs.

Last but not least, we found that although with more unknowns than the LRMs, system with one more target (two-target CPS) in general obtain a better positioning performance than that with less target (one-target CPS) especially when utilizing the LRMs individually rather than collectively. Therefore, when only one type of LRMs (e.g., only ToA or only AoA) is available, a multi-target system can reduce the hardware requirement of the A-agents without much performance loss. This key observation can be considered to guarantee certain positioning performance for device with complexity limitations, since acquiring LRMs from both domain requires a more challenged hardware design. Future work will focus on the performance evaluation at various numbers of both T-agents and moving A-agents.

## REFERENCES


[1] Erisson, "Cellular IoT Evolution for Industry Digitalization," White paper, 2019.

[2] S. Lien, D. Deng, C. Lin, H. Tsai, T. Chen, C. Guo, and S. Cheng, "3GPP NR Sidelink Transmissions Toward 5G V2X," *IEEE Access*, vol. 8, pp. 35 368–35 382, 2020.

[3] 3GPP, TR 38.885 V16.0.0, "Study on NR Vehicle-to-Everything (V2X) (Release 16)," March 2019.

[4] M. Mikami, K. Serizawa, Y. Ishida, H. Nishiyori, K. Moto, and H. Yoshino, "Field Experimental Evaluation on Latency and Reliability Performance of 5G NR V2V Direct Communication in Real Express Highway Environment," in *2020 IEEE 91st Vehicular Technology Conference (VTC2020-Spring)*, 2020, pp. 1–5.

[5] Y. Lu, P. Richter, and E. S. Lohan, "Opportunities and Challenges in the Industrial Internet of Things based on 5G Positioning," in *2018 8th International Conference on Localization and GNSS (ICL-GNSS)*, June 2018, pp. 1–6.

[6] N. Patwari, J. N. Ash, S. Kyperountas, A. O. Hero, R. L. Moses, and N. S. Correal, "Locating the nodes: Cooperative Localization in Wireless Sensor Networks," *IEEE Signal Processing Magazine*, vol. 22, no. 4, pp. 54–69, July 2005.

[7] H. Wymeersch, J. Lien, and M. Z. Win, "Cooperative Localization in Wireless Networks," *Proceedings of the IEEE*, vol. 97, no. 2, pp. 427–450, Feb. 2009.

[8] J. Kulmer, E. Leitinger, S. Grebien, and K. Witrisal, "Anchorless Cooperative Tracking Using Multipath Channel Information," *IEEE Transactions on Wireless Communications*, vol. 17, no. 4, pp. 2262–2275, April 2018.

[9] J. Fink, D. Schaeufele, M. Kasparick, R. L. G. Cavalcante, and S. Stanczak, "Cooperative Localization by Set-theoretic Estimation," in *WSA 2019; 23rd International ITG Workshop on Smart Antennas*, April 2019, pp. 1–8.

[10] 3GPP, TR 38.856 V16.0.0, "Study on local NR positioning in NG-RAN (Release 16)," Dec. 2019.

[11] 3GPP, TS 38.211 V16.1.0, "NR; Physical channels and modulation (Release 16)," March 2020.

[12] 3GPP, TS 38.802 V14.2.0, "Study on New Radio Access Technology, Physical Layer Aspects (Release 14) ," Sep. 2017.

[13] S. Sand, A. Dammann, and C. Mensing, *Positioning in Wireless Communication Systems*. John Wiley & Sons Ltd., June 2014.

[14] D. Simon, *Optimal State Estimation: Kalman, H Infinity, and Nonlinear Approaches*. New York, NY, USA: Wiley-Interscience, 2006.

[15] Y. Lu, M. Koivisto, J. Talvitie, M. Valkama, and E. S. Lohan, "EKF-based and geometry-based positioning under location uncertainty of access nodes in indoor environment," in *2019 International Conference on Indoor Positioning and Indoor Navigation (IPIN)*, Sep. 2019, pp. 1–7.

[16] Wireless Insite, "https://www.remcom.com/wireless-insite-em-propagation-software," Remcom Incooperation.

[17] E. Hyytiä, H. Koskinen, P. Lassila, A. Penttinen, J. Virtamo, and J. Roszik, "Random Waypoint Model in Wireless Networks," *Networks and Algorithms: Complexity in physics and Computer Science*, Jan. 2005.

[18] 3GPP, TS 22.261 V17.2.0, "Service requirements for the 5G system; Stage 1 (Release 17)," March 2020.